Revista Mexicana de Astronomía y Astrofísica, **59**, 105–112 (2023)

https://doi.org/10.22201/ia.01851101p.2023.59.01.07

REFRACTION OF A HERBIG-HARO JET TRAVELLING THROUGH A SHEAR LAYER

A. C. Raga[1], A. Castellanos-Ramírez[2], and J. Cantó[2]

Received June 27 2022; accepted October 21 2022

ABSTRACT

We study the problem of a radiative Herbig-Haro (HH) jet which travels through a slip surface into a region of side-streaming environment. The interaction with the streaming environment produces an oblique shock that deflects the jet beam. A simple, analytic model for this shock gives the jet deflection as a function of the incidence angle and the environment-to-jet ram pressure ratio. We find that in the case of higher environmental ram pressure, for a high enough incidence angle, the jet stalls and does not penetrate substantially into the streaming environment. We present 3D gas dynamic simulations illustrating the jet deflection and stalling regimes. Possible applications to HH jets showing sudden deflections in their propagation are discussed.

RESUMEN

Estudiamos el problema de un jet Herbig-Haro (HH) radiativo que pasa a través de una superficie de contacto a una región de medio ambiente en movimiento lateral. La interacción con el medio ambiente en movimiento produce un choque oblicuo que deflecta el haz del jet. Un modelo analítico sencillo para este choque da la deflección del jet en función del ángulo de incidencia y del cociente de presiones hidrodinámicas entre el medio ambiente y el jet. Encontramos que en el caso de medio ambiente con mayor presión hidrodinámica, para un ángulo de incidencia suficientemente alto el jet se estanca, y no penetra sustancialmente dentro del medio ambiente en movimiento. Presentamos simulaciones hidrodinámicas 3D que ilustran los regímenes de deflección y de estancamiento. Se discuten posibles aplicaciones a jets HH que muestran deflecciones repentinas en su propagación.

Key Words: ISM: jets and outflows — ISM: kinematics and dynamics — stars: pre-main-sequence — stars: winds, outflows

1. INTRODUCTION

Herbig-Haro (HH) jets sometimes show sudden changes of direction, which have been generally attributed to collisions with dense obstacles. The best studied example of this effect is the HH 110 outflow.

HH 110 was discovered by Reipurth & Olberg (1991). It was soon realized that this object corresponds to a jet which becomes brighter and less collimated after a sudden change in direction (Reipurth et al. 1996; Rodríguez et al. 1998). Proper motions (e.g., Kajdic et al. 2012) and spatially resolved spectroscopy (e.g., Riera et al. 2003; López et al. 2010) can be interpreted in this jet deflection context. This object has even been compared to laboratory experiments of jets deflected by collisions with an obstacle (Hartigan et al. 2009).

Though HH 110 is the most notable example, qualitatively similar situations are found in regions with high spatial concentrations of YSO outflows. For example, Walawander et al. (2005) found some notable deflected jets in the Perseus molecular cloud, and Hayashi & Pyo (2009) in the L1551 dark cloud. These objects mostly await more detailed studies.

Raga & Cantó (1995) modeled analytically and numerically (with 2D gas dynamics) the initial deflection of a jet by an oblique collision with a dense obstacle, and suggested that HH 110 might correspond to such a flow. However, at later times the jet penetrates the cloud, and has a curved trajectory before reemerging (Raga & Cantó 1996), not

[1]Instituto de Ciencias Nucleares, UNAM, México.
[2]Instituto de Astronomía, UNAM, México.

resembling HH 110. 3D simulations of this type of jet/cloud interaction were presented by de Gouveia Dal Pino (1999) and Raga et al. (2002).

In the present paper, we study the passage of a jet through a slip boundary, in which the environment is stationary (with respect to the jet source) on one side, and in supersonic sideways motion on the other side. This situation could represent a jet impacting on a supersonically travelling cloud (which would be a reasonable scenario in a region with supersonic turbulence), or on material disturbed by the previous passage of another YSO outflow.

We first present analytic considerations for evaluating the deflection of the jet as a function of the environment/jet ram pressure balance ratio p and the incidence angle ϕ of the interaction (§ 2). Finding that there are two regimes (a jet deflection and a stagnation case), we then compute two 3D simulations illustrating the very different resulting flows (§ 3). The results are summarized in § 4, and we discuss the possible application of these models to observed deflected HH jets in § 5.

2. ANALYTIC CONSIDERATIONS

Let us consider the problem of a steady jet flow emerging from a stationary environment into a region with a moving environment. For the sake of simplicity, we assume that the jet emerges at an angle ϕ with respect to the (infinitely narrow) environmental velocity shear surface, and that the plane containing the jet and the environmental velocities is perpendicular to this shear surface. This situation is shown schematically in Figure 1.

In a cut through the midplane of the flow, two oblique shocks are formed: one of them refracting the jet beam, and the other one deflecting the flowing environment. These shocks lie at angles β and α, respectively, with respect to the environmental shear layer (see Figure 1). The velocities behind these two shocks (v_{jr} and v_{ar}) are parallel, forming a deflected environment/jet flow. For the case of a 2D problem, the two shocks are straight, and we will assume that this is also a reasonable approximation for the mid-plane of a cylindrical jet/plane shear layer interaction.

The postshock flow velocities form angles α_1 and $\beta_1 >$ with the shock surfaces. The tangents of these angles are inversely proportional to the compression in each shock, so that for the highly radiative HH flow case (in which the compressions have typical values of ≈ 100) they will have values $\ll 1$. It is therefore a good approximation to set $\alpha \approx \beta$ (see Figure 1).

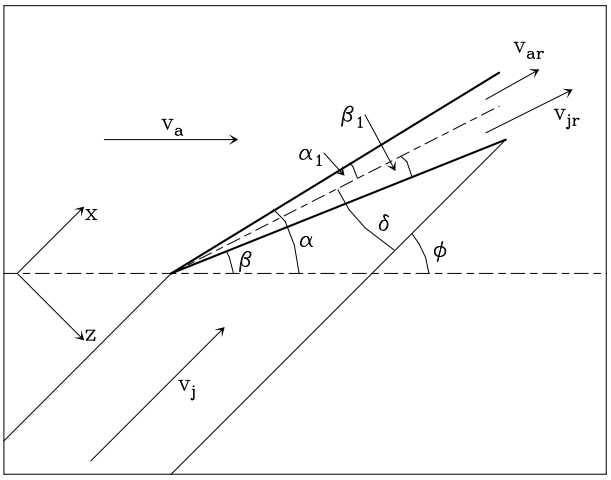

Fig. 1. Schematic diagram showing an interface (dashed horizontal line) between a stationary environment (below) and a streaming environment (above) of velocity v_a. A jet (of velocity v_j impacts on the interface at angle ϕ. Two shocks are formed: one that deflects the jet (at an angle β to the interface) and a second one that deflects the environment (at an angle α). The contact discontinuity separating the deflected jet and environmental gas lies in between these two shocks. The deflected environment has a velocity v_{ar} and the deflected jet a velocity v_{jr}, both parallel to the shocked environment/jet contact discontinuity. The jet beam goes through a deflection $\delta = \phi - \alpha$. The xz-reference system used in the numerical simulations (in which the jet travels along the x-axis) is shown with the arrows in the center left region of the schematic diagram.

With this condition, the balance between the two post (strong) shock pressures is:

$$\rho_j v_{jn}^2 = \rho_a v_{an}^2 \,, \tag{1}$$

$$\rightarrow \sin^2(\phi - \alpha) = p^2 \sin^2 \alpha \,, \tag{2}$$

with

$$p = \sqrt{\frac{\rho_a}{\rho_j}} \frac{v_a}{v_j} \,, \tag{3}$$

where ρ_j and ρ_a are the densities and v_j and v_a the velocities (with components normal to the shocks v_{an} and v_{jn}) of the jet and the environment, respectively. Clearly, p is the square root of the environment-to-jet ram pressure ratio. From equation (2) we then obtain the shock angle α as a function of the incidence angle ϕ:

$$\tan \alpha = \frac{\sin \phi}{p + \cos \phi} \,. \tag{4}$$

In the α_1, $\beta_1 \ll 1$ high compression approximation, the deflection angle between the impinging (v_j)

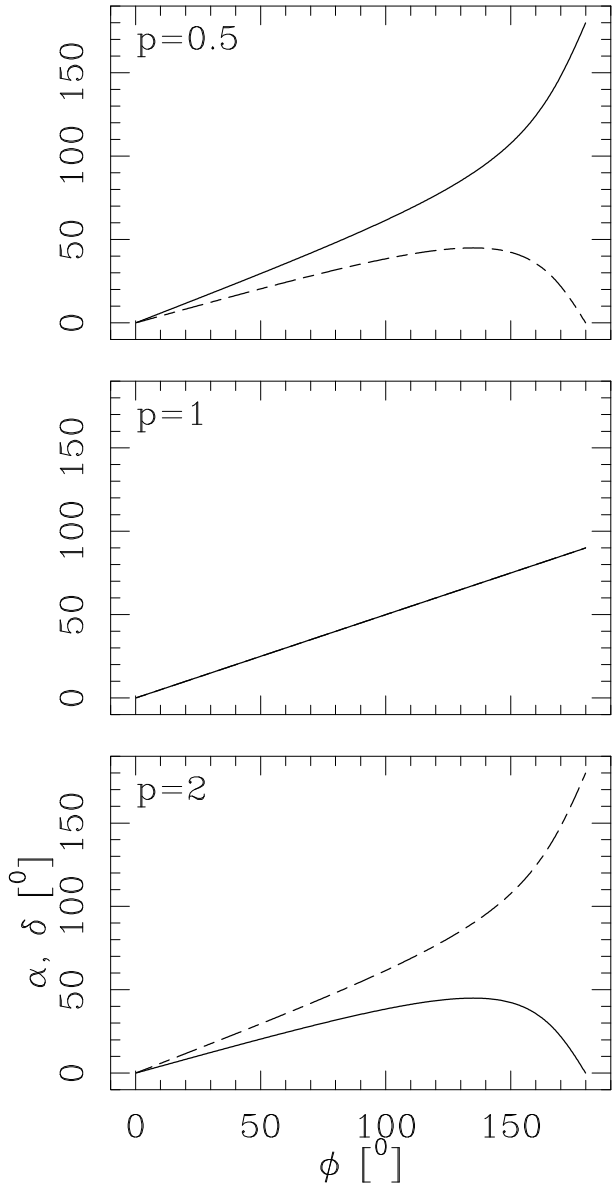

Fig. 2. The α (solid lines) and δ (dashed line) angles (i.e., the angle of the jet shock with respect to the environmental shear layer and the jet deflection angle, respectively, see Figure 1) as a function of the incidence angle ϕ. The results shown in the three frames correspond to $p = 0.5$, 1 and 2 (see equation 3). For $p = 1$, α and ϕ coincide.

and refracted (v_{jr}) jet velocities is $\delta = \phi - \alpha$ (see Figure 1). Using equation (2) we then obtain:

$$\tan\delta = \frac{\sin\phi}{1/p + \cos\phi}\,. \tag{5}$$

The shock angle α and the deflection angle δ (equations 2 and 5, respectively) are shown as a function of p and ϕ (see equation 3) in Figure 2. Using equation (5) we can now calculate the velocity of the deflected jet:

$$v_{jr} = v_j \cos\delta\,, \tag{6}$$

see Figure 1.

It is clear that α and δ switch their values under a $p \to 1/p$ transformation (see equations 4 and 5), as can be seen in Figure 2. This property is an expected result due to the symmetry of the jet/streaming environment interaction (see Figure 1).

Also, the $p = 1$ case (equal jet and environmental ram pressures, see equation 3) produces the straightforward result:

$$\delta = \alpha = \phi/2\,, \tag{7}$$

deduced from equations (4-5).

In Figure 3, we show α (or δ) for a number of different p (or $1/p$) values. Two families of solutions (having values of either 1 or 0 for $\phi = 180°$) are separated by the linear, $p = 1$ solution (see equation 7).

It is clear that for $p < 1$ there is a maximum possible value δ_m for the jet deflection (see Figures 2 and 3). From equation (5) it is straightforward to show that this maximum occurs for an incidence angle

$$\cos\phi_m = -p\,, \tag{8}$$

and has a maximum deflection

$$\tan\delta_m = \frac{p}{\sqrt{1-p^2}}\,. \tag{9}$$

Figure 4 shows these two angles as a function of p.

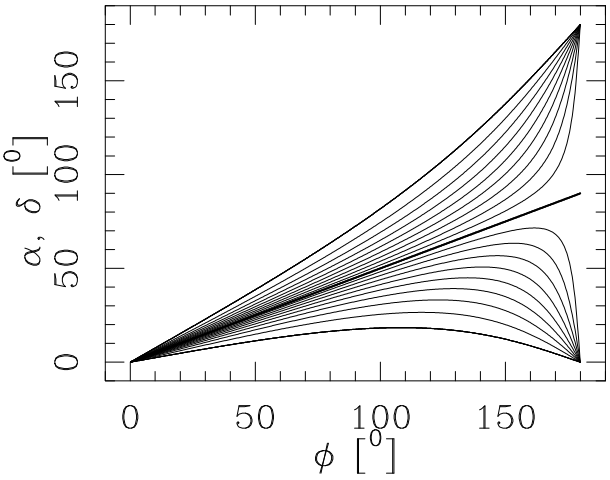

Fig. 3. The displayed curves correspond to α as a function of ϕ for p = 0.1, 0.2, ... 1, 1/0.9, 1/0.8, 1/0.7, ... 1/0.1 for (top to bottom curves) or to δ as a function of ϕ for $1/p$ = 0.1, 0.2, ... 1, 1/0.9, 1/0.8, 1/0.7, ... 1/0.1 (top to bottom curves). The thick, central straight line is the $p = 1$ solution.

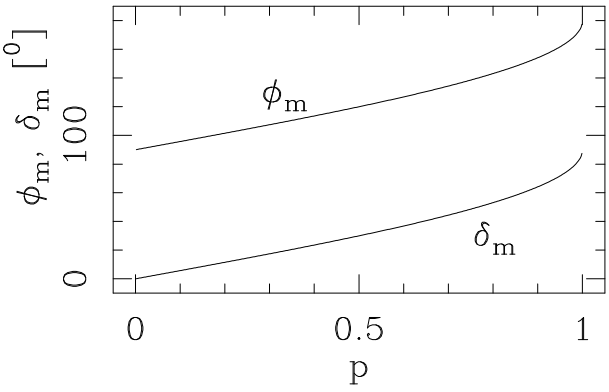

Fig. 4. Maximum jet deflection angle δ_m and incidence angle ϕ_m at which the maximum deflection occurs as a function of p.

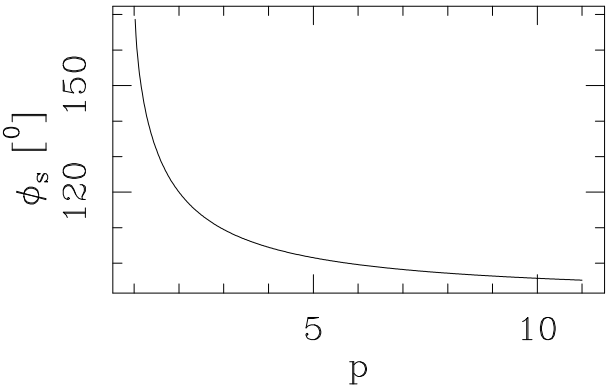

Fig. 5. Incidence angle for jet stagnation ϕ_s as a function of p.

Another interesting feature of the jet deflection is that for $p > 1$ one can have $\delta > 90°$. For

$$\cos\phi_s = -1/p\,, \tag{10}$$

the jet flow has a stagnation ($\delta = 90°$) at a shock perpendicular to the jet flow (this result being straightforwardly obtained from equation 5). Figure 5 shows ϕ_s as a function of p.

For $\phi > \phi_s$, we have deflections $\delta > 90°$. This corresponds to a regime in which the jet is deflected into a direction that goes against the streaming environment. Because this occurs only in the $p > 1$ regime of high environmental ram pressure, this deflected material will quickly slow down and remain close to the jet/streaming environment interaction region. This "stalled jet" regime is explored below with a gas dynamic simulation.

Finally, we note that the mixed jet/streaming environment flow emerging from the two-flow interaction region has an environment to jet mass ratio

$$r_{aj} = \frac{\rho_a v_{an}}{\rho_j v_{jn}} = \sqrt{\frac{\rho_a}{\rho_j}}\,, \tag{11}$$

the second equality being a direct result of the ram-pressure balance condition (see equation 1). As the flow travels away from the interaction region (shown in Figure 1), more environmental mass is incorporated into the beam of the curved flow.

3. NUMERICAL SIMULATIONS

3.1. *The Two Computed Models*

In order to illustrate the general characteristics of jet flows interacting with an environmental velocity shear, we have calculated two models:

- M1: a cylindrical jet with initial radius $r_j = 10^{16}$ cm, density $n_j = 10^3 \mathrm{cm}^{-3}$, temperature $T_j = 100$ K and velocity $v_j = 100$ km s^{-1} emerging from a stationary environment of density $n_b = 500$ cm^{-3} and temperature $T_b = 200$ K into a flowing medium of velocity $v_a = 30$ km s^{-1} (with a density $n_a = 10^3$ cm^{-3} and temperature $T_a = 100$ K) at an incidence angle $\phi = 60°$.
- M2: the same jet, but emerging from a stationary environment of density $n_b = 500$ cm^{-3} and temperature $T_b = 200$ K into a flowing medium of velocity $v_a = 50$ km s^{-1} with a density $n_a = 10^4$ cm^{-3} and temperature $T_a = 10$ K at an incidence angle $\phi = 150°$.

For model M1, the p parameter (the square root of the streaming environment to jet ram pressure ratio, see equation 3) is $p_1 = 0.3$. From Figure 3, we see that for this value of p and for the $\phi = 60°$ incidence angle of this model, we expect a jet deflection of $\approx 30°$.

For model M2, we have a p parameter $p_2 = 1.58$. From Figure 5, we see that for this value of p, the minimum incidence angle for jet stagnation has a $\phi_s \approx 129°$, so that the $\phi = 150°$ incidence angle of this model should lead to the formation of a stagnated jet flow.

3.2. *The Numerical Setup*

We have used a 3D version of the yguazú-a code (described in detail by Raga et al. 2000, and extensively used over the last two decades) with a 5-level binary adaptive grid of maximum resolution $= 3.9 \times 10^{14}$ cm along the three Cartesian axes. This results in a resolution of the jet diameter with ≈ 51 grid points.

In the two simulations, the jet is injected along the x-axis, and the environment has two regions, an upper one of density n_a, temperature T_a and velocity

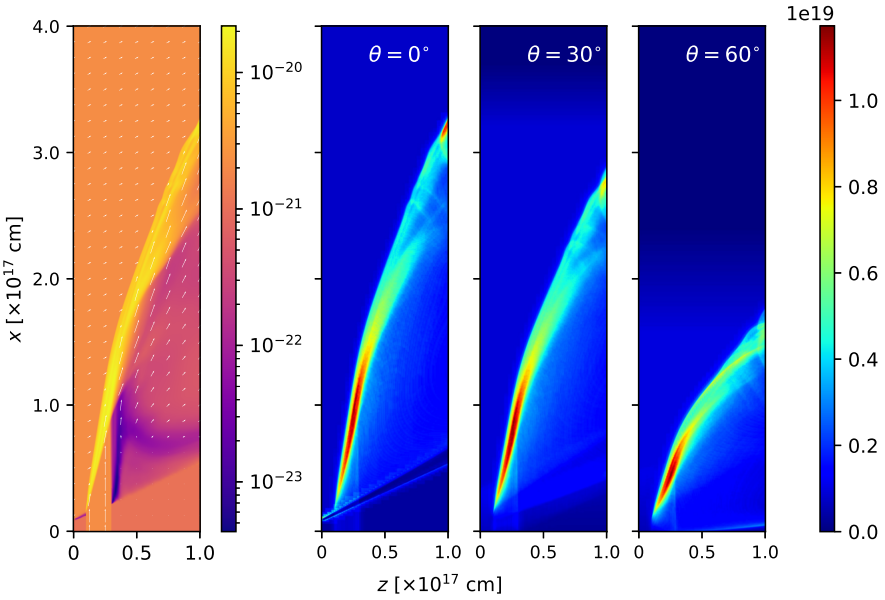

Fig. 6. Results obtained for model M1 (see the text) after a $t = 2000$ yr time-integration. The left panel shows the zx-midplane density map (given in g cm^{-3} by the bar at the right of the frame), and (white) arrows with lengths and directions corresponding to the local flow velocities. The three right panels show column density maps (given in 10^{19} cm^{-2} by the bar at the right) computed assuming $\theta = 0$, 30 and 60° angles between the x-axis and the plane of the sky (as shown on the top of the three panels). The z- and x-axes are given in units of 10^{17} cm. The color figure can be viewed online.

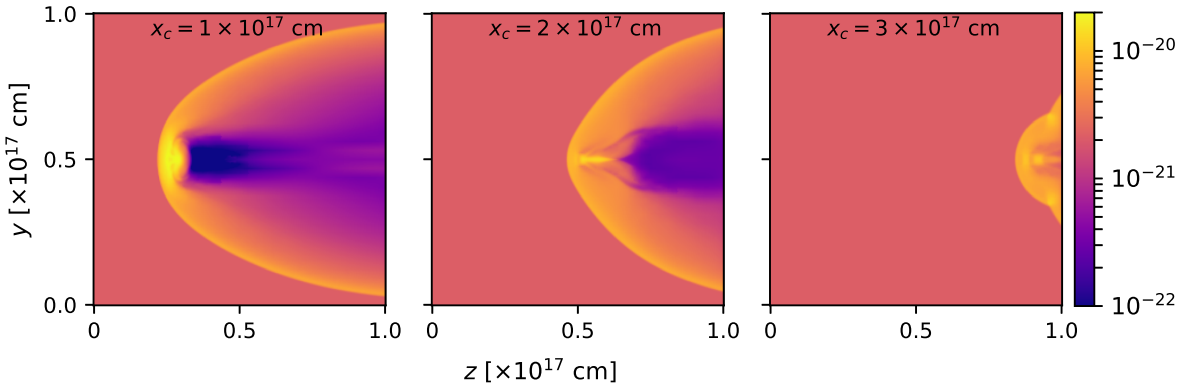

Fig. 7. Results obtained for model M1 (see the text) after a $t = 2000$ yr time-integration. The three panels show the density stratifications on yz-cuts (see Figure 6) at three different values of x (1, 2 and 3×10^{17} cm), as labeled on the top of each frame). The color figure can be viewed online.

v_a (in the xz-plane) directed obliquely at an angle of $90 - \phi$, anticlockwise with respect to the z-axis (where ϕ is the incidence angle of the jet with respect to the environmental velocity slip line). Therefore, the velocity shear region separating the lower (stationary) and upper (moving) regions of the environment is parallel to the y-axis and inclined on the xz-plane.

In the simulations, inflow boundaries are applied on the yz-plane within the $r_j = 10^{16}$ cm cylindrical jet beam and along the $z = 0$ plane, where the flowing environment is injected in the upper region of the domain. The remaining edges of the computational domain are treated as outflow boundaries.

The gas dynamic code integrates the continuity equation, the three momentum and the energy equa-

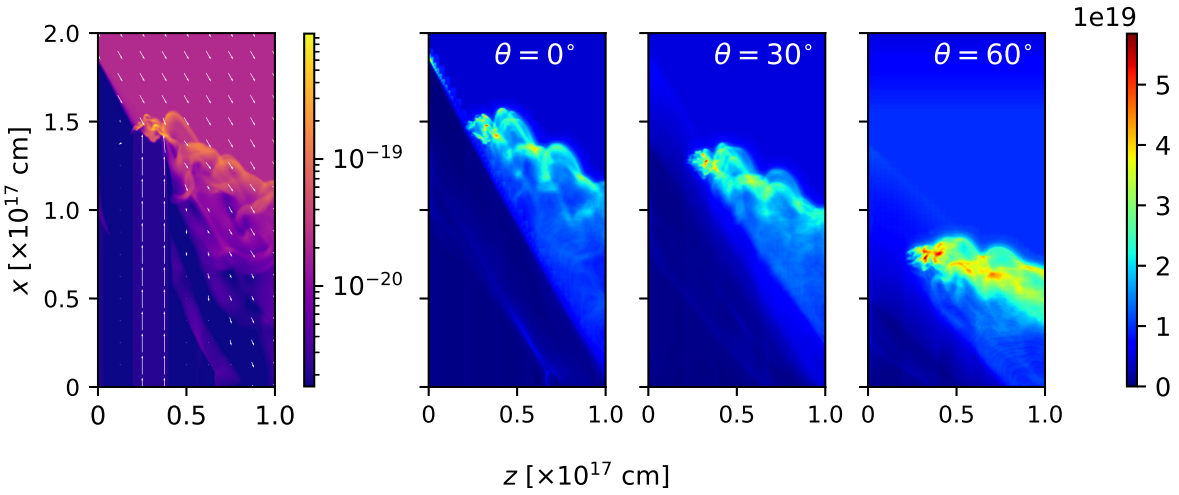

Fig. 8. The same as Figure 6 but for model M2. The color figure can be viewed online.

tions, together with a rate equation for neutral H (which includes collisional ionization and radiative recombination). The parametrized cooling rate of Raga et al. (2002) is included in the energy equation. The gas in all of the computational domain is initially neutral, with a seed electron density coming from singly ionized C, allowing the gas to become collisionally ionized in the hot, post-shock regions.

The simulations are started with the jet beam in contact with the slip boundary, and are integrated in time until an approximately stationary flow configuration is obtained. The resulting flows are presented in the following subsection.

3.3. *The Deflected Jet and the Stalled Jets*

Figure 6 shows the flow resulting from model M1 after a 2000 yr time-integration. The first panel shows an xz-cut through the middle of the jet beam, displaying the density stratification and the flow field. The other three panels show the column density calculated for three orientations ($\theta = 0$, 30 and 60°) between the z-axis and the plane of the sky.

We find that the jet shows the deflection shock of our analytic model, and that after the end of the deflection shock, the locus of the jet beam curves due to the ram pressure of the streaming environment, The column density maps (three right panels of Figure 6) show that the deflected flow has a curved, collimated jet morphology for all chosen orientation angles (including the more head-on, $\theta = 60°$ observational perspective).

The curved jet beyond the deflection shock is the jet/sidewind interaction regime that has been studied by Cantó & Raga (1995), in which the jet develops a "plasmon shaped" cross section. This plasmon cross section is seen in the yz-density cuts shown in Figure 7, corresponding to planes perpendicular to the initial direction of the jet flow.

Figure 8 shows the flow resulting from model M2 after a 2000 yr time-integration. The mid-plane density stratification shows that the jet terminates at a shock with a complex, time-dependent shape. The post-shock material forms a series of clumps or eddies that are advected by the impinging environment, forming a turbulent trail.

The column density maps show that this turbulent trail has a complex 3D structure, with considerably higher column densities when observed in more head-on directions (see the $\theta = 60°$ frame of Figure 8). The complexity of the structure is illustrated by the yz-density cut (taken at $x = 1.38 \times 10^{17}$ cm) shown in Figure 9.

4. SUMMARY

We developed an analytic model (§ 2) of a radiative jet going through an environmental shear surface. We obtain a full solution in the limiting case of high compression in the two radiative shocks produced in the interaction.

For given values of the dimensionless parameter p (equal to the square root of the streaming environment to jet ram-pressure ratio, see equation 3), we find expressions for the jet deflection angle δ (see equation 5) and the angle α between the interaction shocks and the environmental shear surface (see equation 4) as a function of the incidence angle ϕ (see Figures 1, 2 and 3).

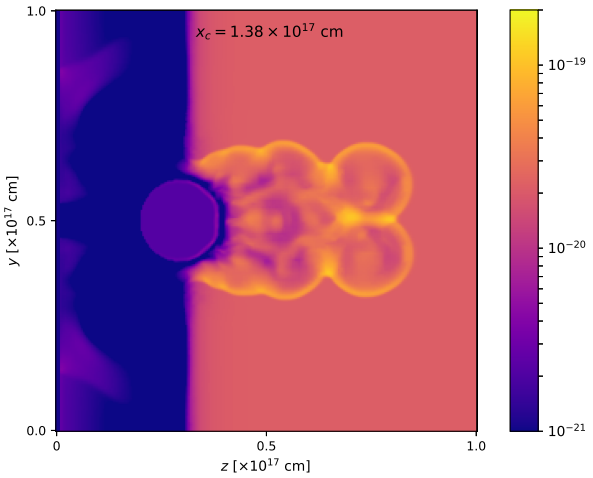

Fig. 9. Density yz-cut at $x = 1.38 \times 10^{17}$ cm obtained from model M2 (see the text) after a $t = 2000$ yr time-integration. The color figure can be viewed online.

Two interesting results are that:

- for $p < 1$ (higher jet ram-pressure), there is a maximum possible jet deflection angle δ_m (given as a function of p by equation 9, and shown in Figure 4);

- for $p > 1$ (higher environmental ram-pressure), one has deflections $\delta > 90°$ (i.e., the jet is deflected in a direction against the flowing environment) for incidence angles $\phi > \phi_s$ (with ϕ_s given by equation 10, and shown in Figure 5 as a function of p).

The interactions with $\phi > \phi_s$ correspond to stalled jets, in which the post-interaction shock jet is stopped and then entrained by the streaming environment.

In order to illustrate the "deflected" and "stalled" jet interaction regimes, we computed two 3D simulations with values of p (see equation 3) and incidence angle ϕ (see Figure 1) clearly placing the flows in each of these two regimes. These simulations are described in § 3, and the results are shown in Figures 6-9.

We find that:

- the deflected jet regime leads to a clean deflection of the jet beam (from a vertical, to an oblique direction in the panels of Figure 6), and at larger distances (beyond the end of the jet deflection shock) by a curved jet locus resulting from the continuing interaction of the deflected jet with the streaming environment;

- the stalled jet regime shows an abrupt end of the jet flow at the position of the environmental shear, followed by a turbulent structure in which the stalled jet material is incorporated into the environmental flow (see Figures 8 and 9).

We are not aware of an observed HH jet deflection that could be in this latter regime.

5. CONCLUSIONS

We have presented analytic and numerical models for a radiative jet that travels through an environmental shear surface, which divides an internal region around the jet source (which shares the motion of the jet source) and an external region with a non-zero velocity (with respect to the jet source).

This flow configuration could correspond to different situations. For example:

- the case of an internal region that is denser than the external region could correspond to a jet emerging from a dense core (containing the jet source) into a lower density, streaming environment;

- the case of a lower density internal region and a denser external region could correspond to a narrow jet meeting a broader outflow (e.g., a spatially extended molecular outflow), or a dense cloud in motion relative to the jet source.

These two cases are relevant for regions with many bipolar jet systems, such as the L1551 cloud (e.g., Hayashi & Pyo 2009), the Perseus molecular cloud (Walawander et al. 2005) and NGC 1333 (Raga et al, 2013), some of which show several jets with sudden changes in projected direction. Both jet-cloud and jet-molecular outflow collisions are possibly occurring.

Our present model is also relevant for the case of the remarkable HH 110 deflected jet system (e.g., Kajdic et al. 2012). This object has been modeled as an oblique collision of a jet with a dense cloud (e.g., de Gouveia Dal Pino 1999; Raga & Cantó 2005). Raga et al. (2002) carried out a more extended numerical exploration of the jet/cloud collision problem and obtained deflected jets that qualitatively resemble HH 110. They noted, however, that for reasonable jet/cloud density contrasts it was not possible to maintain the jet deflection at the cloud surface for a long enough timescale, as the jet starts boring through the cloud.

The addition of a relative motion between the jet source and the cloud directly solves this problem. The models of the present paper show that this

relative motion results in an approximately stationary jet deflection, which will last until the collision region reaches the edge of the cloud. The relative jet source/cloud motion is probably the missing element in all of the models that have been previously calculated for the HH 110 flow.

This work was supported by the DGAPA (UNAM) grant IG100422. A. Castellanos-Ramírez acknowledges support from a CONACyT postdoctoral fellowship, and the resources on the Miztli supercomputer obtained through the project LANCAD-UNAM-DGTIC-408. We thank an anonymous referee for helpful comments that gave rise to figures 7 and 9, equation 11, and modifications throughout the paper.

REFERENCES

de Gouveia Dal Pino, E. M. 1999, ApJ, 526, 862, https://doi.org/10.1086/308037

Hartigan, P., Foster, J. M., Wilde, B. H., et al. 2009, ApJ, 705, 1073, https://doi.org/10.1088/0004-637X/705/1/1073

Hayashi, M. & Pyo, T.-S. 2009, AJ, 694, 582, https://doi.org/10.1088/0004-637X/694/1/582

Kajdiĉ, P., Reipurth, B., Raga, A. C., Bally, J., & Walawender, J. 2012, AJ, 143, 106, https://doi.org/10.1088/0004-6256/143/5/106

López, R., García-Lorenzo, B., Sánchez, S. F., et al. 2010, MNRAS, 406, 2193, https://doi.org/10.1111/j.1365-2966.2010.16831.x

Raga, A. C. & Cantó, J. 1995, RMxAA, 31, 51

_____. 1996, MNRAS, 280, 567, https://doi.org/10.1093/mnras/280.2.567

Raga, A. C., Navarro-González, R., & Villagrán-Muniz, M. 2000, RMxAA, 36, 67

Raga, A. C., de Gouveia Dal Pino, E. M., Noriega-Crespo, A., Minini, P. D., & Velázquez, P. F. 2002, A&A, 392, 267, https://doi.org/10.1051/0004-6361:20020851

Raga, A. C., Noriega-Crespo, A., Carey, S. J., & Arce, H. G. 2013, ApJ, 145, 28, https://doi.org/10.1088/0004-6256/145/2/28

Reipurth, B. & Olberg, M. 1991, A&A, 246, 535

Riera, A., Raga, A. C., Reipurth, B., et al. 2003, AJ, 126, 327, https://doi.org/10.1086/375759

Rodríguez, L. F., Reipurth, B., Raga, A. C., & Cantó, J. 1998, RMxAA, 34, 69

Walawander, J., Bally, J., & Reipurth, B. 2005, AJ, 129, 2308, https://doi.org/10.1086/428955

J. Cantó & A. Castellanos-Ramírez: Instituto de Astronomía, Universidad Nacional Autónoma de México, Ap. 70-468, 04510 CDMX, México.

A. C. Raga: Instituto de Ciencias Nucleares, Universidad Nacional Autónoma de México, Ap. 70-543, 04510 CDMX, México (raga@nucleares.unam.mx).